SCIENCE CHINA Materials LETTERS

mater.scichina.com link.springer.com

Published online 17 July 2020 | https://doi.org/10.1007/s40843-020-1396-7
Sci China Mater 2020, 63(11): 2351–2357

Plasma-regulated N-doped carbon nanotube arrays for efficient electrosynthesis of syngas with a wide CO/H_2 ratio

Yan Ji[1], Yanmei Shi[1*], Cuibo Liu[1] and Bin Zhang[1,2*]

Syngas, a mixture of CO and H_2 with a specific ratio, is of great necessity for the industrial production of olefins, liquid fuels, polymers, and drugs [1–4]. Currently, syngas is mainly acquired under harsh conditions from the gasification of solid coal and petroleum coke, as well as the steam reforming of natural gas [5,6], which accelerate the energy crisis and aggravate CO_2 emission. Electrochemical CO_2 reduction reaction (CO_2RR) is considered to be a promising strategy to solve these problems [7,8]. Although the conversion of CO_2 to multicarbon products is still elusive, electrocatalysts towards CO are extensively studied [9–15]. By adjusting the reaction rates of CO_2RR to CO and the competing hydrogen evolution reaction (HER), the syngas with a controllable ratio of CO/H_2 can be obtained under mild conditions [16,17].

Carbon materials are among the well-established electrocatalysts for CO_2RR, because of their excellent conductivity, chemical stability, and abundant active sites [18]. Though the intrinsic activity of carbon materials is poor, the introduction of heteroatoms (N, S, B, etc.) can effectively promote their electrochemical activity and selectivity [19–23]. Taking N-doped carbon materials as the examples, the doping N atoms exist in the forms of pyridinic N, pyrrolic N, graphitic N, and oxidized N in the carbon materials. With different N-doping forms, the corresponding electrochemical CO_2RR performance may exhibit a huge difference [24,25]. For instance, recent studies showed that pyridinic N atoms were more likely to adsorb CO_2 and serve as the favorable sites for CO_2RR [26–28]. Accordingly, the CO_2RR performances can be manipulated by regulating the component of the carbon materials.

Plasma treatment has recently emerged as a promising technology for surface modification and material synthesis in the field of electrocatalysis [29–31]. Plasma is the fourth state of matter composed of molecules, radicals, ions, and atoms with equal positive and negative charges [32]. Under sufficient energy (such as electric discharge), plasma is generated from argon, oxygen, etc. to produce charged particles bombarding the sample for cleaning, etching, or exfoliation [33]. Plasma treatment could be conducted at room temperature without producing chemical wastes and changing the main structure of the materials [34,35]. By optimizing the operating condition, plasma treatment will be an attractive strategy to regulate the component of carbon materials in a facile way.

Here, we present the synthesis of syngas with a controllable ratio of CO/H_2 by electrochemical CO_2RR over Ar-plasma-treated N-doped carbon nanotube arrays (pCNTA, Fig. 1a). The component of the N-doped carbon nanotube arrays (CNTA) is regulated by Ar-plasma treatment. And the CO Faradaic efficiency (FE) of the optimized sample reaches up to 75% with the stability for over 10 h. With different conditions of plasma treatment, the ratio of CO/H_2 can be adjusted from 0.55 to 3.03, which is appropriate for the typical downstream Fischer-Tropsch synthesis.

The CNTA is prepared by a facile two-step strategy (see more details in the Experimental section and Fig. S1, Supplementary information). Under the observation of a scanning electron microscope (SEM), the as-prepared CNTA demonstrates the homogeneous nanowire arrays with the length of several micrometers grown compactly on the substrate (Fig. S2). A closer look at the CNTA shows the nanowires are slightly curled with a diameter of about 100 nm (Fig. 1b). The transmission electron mi-

[1] Department of Chemistry, School of Science, Institute of Molecular Plus, Tianjin University, Tianjin 300072, China
[2] Tianjin Key Laboratory of Molecular Optoelectronic Science, Collaborative Innovation Center of Chemical Science and Engineering, Tianjin 300072, China
* Corresponding authors (emails: bzhang@tju.edu.cn (Zhang B); yanmeishi@tju.edu.cn (Shi Y))

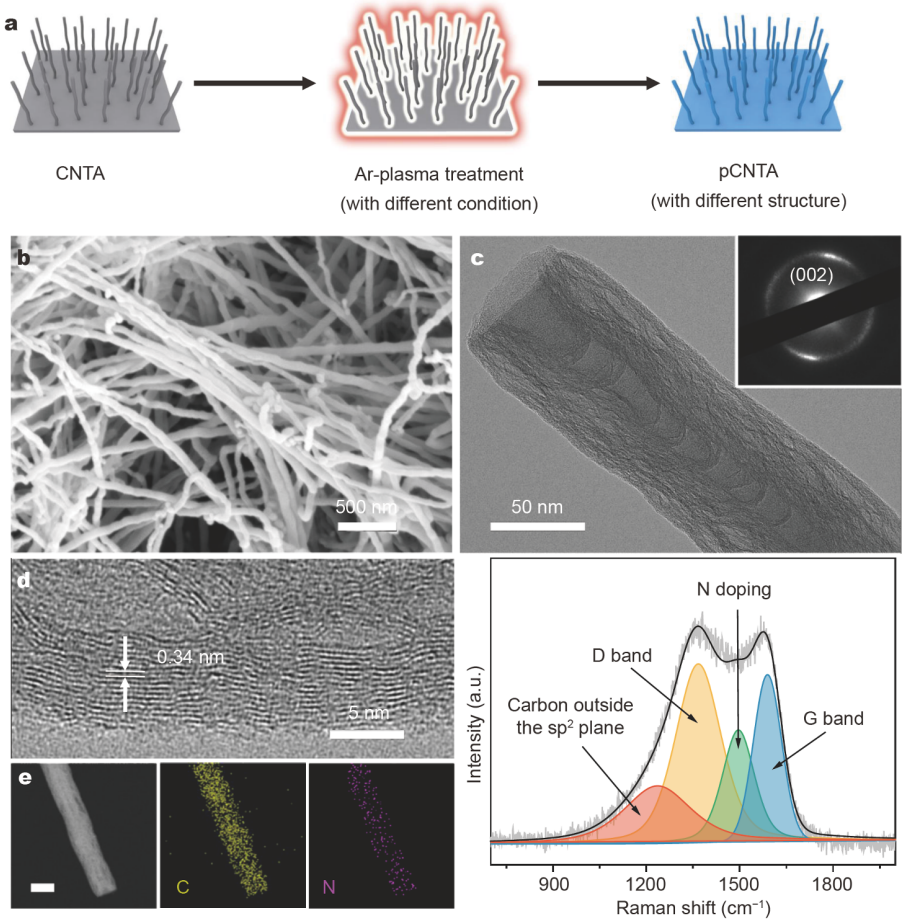

Figure 1 (a) Illustration of the preparation of pCNTA. (b) SEM image, (c) TEM image, (d) HRTEM image, (e) Scanning TEM and elemental distribution mapping images, and (f) Raman spectra of the as-prepared CNTA. The inset in (c) is the corresponding SAED pattern. The scale bar in (e) is 100 nm.

croscopy (TEM) image of the CNTA exhibits a multiwall nanotube structure (Fig. 1c). The ring in the corresponding selected area electron diffraction (SAED) pattern matches well with the (002) plane of a CNT (inset Fig. 1c). The high-resolution TEM (HRTEM) image shows the interlamellar spacing of 0.34 nm (Fig. 1d), which is in accordance with the layer distance of single-layer graphene [36]. Elemental distribution mapping images of the as-prepared CNTA indicate that the sample is composed of C and N, both of which distribute uniformly on the whole nanotube (Fig. 1e). The result of the elemental analyzer shows that the percentage of N in CNTA is ~15%. These results illustrate that the N-doped multiwall CNTA is successfully prepared. Then Raman spectroscopy was employed to further investigate the structure of CNTA. As shown in Fig. 1f, four bands can be deconvoluted from the Raman spectrum of CNTA. Besides the well-known D band at 1350 cm^{-1} and G band at 1600 cm^{-1}, bands at 1200 and 1510 cm^{-1} are also found to reflect the carbon atoms outside the perfect sp^2 plane like aliphatic hydrocarbons or amorphous structure, and the distorted structure such as the doping of heteroatoms [37,38], respectively, indicating the as-prepared CNTA is quite disordered.

Then, Ar-plasma treatment with different conditions was conducted on the CNTA. As shown in Fig. 2a and Fig. S3, nearly no morphological change appears in the pCNTA*n* (*n* represents the treatment time). The result of the elemental analyzer shows that within 10-min plasma treatment, the percentage of C and N in the pCNTA changes little (Fig. 2b). If the treatment time is longer than 10 min, both the contents of C and N begin to decrease in proportion to the treatment time. In the C 1s X-ray photoelectron spectra (XPS) of the as-prepared CNTA, the peaks at 284.3, 285.1, and 286.3 eV are attributed to C=C, C–C, and C–N/C–O, respectively [39–

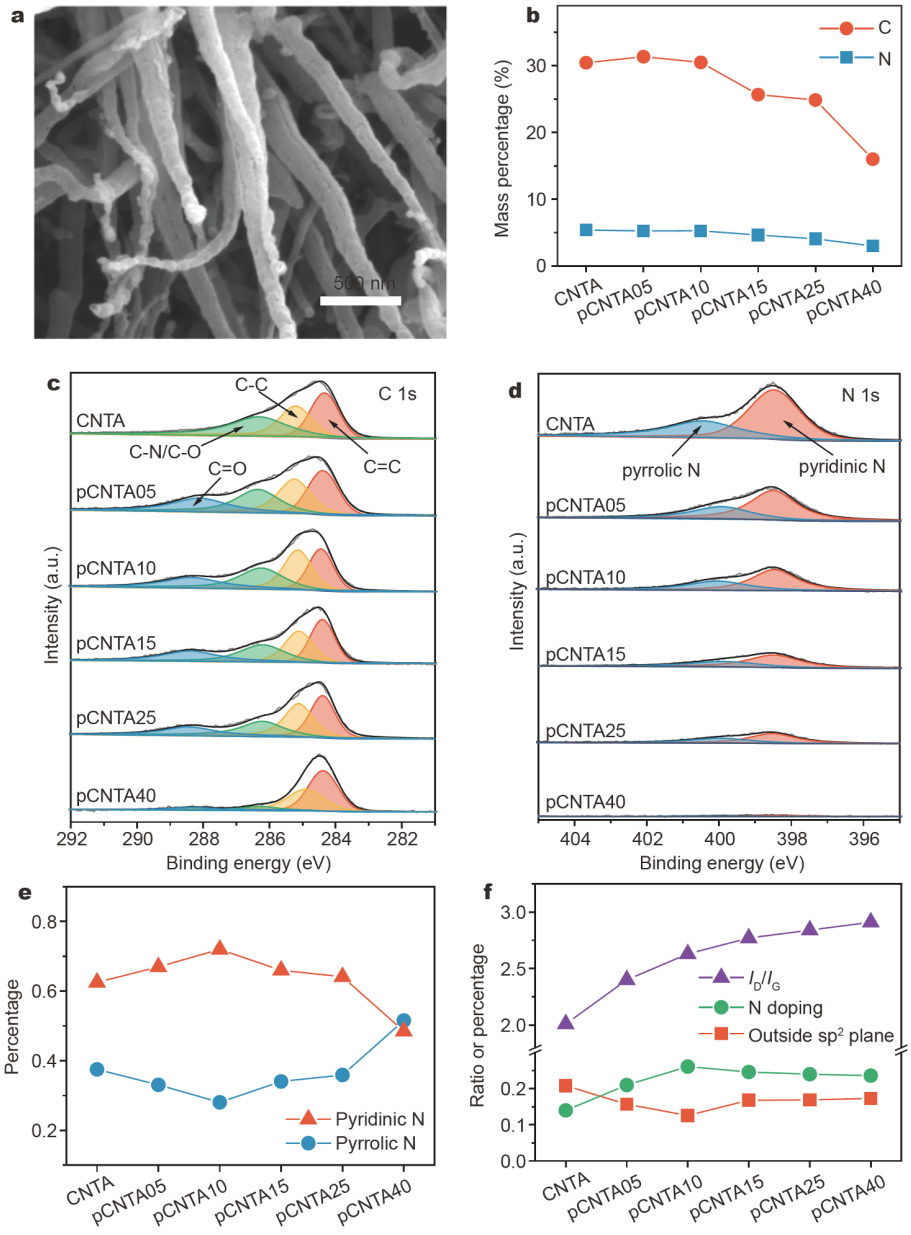

Figure 2 (a) SEM image of pCNTA. (b) Elemental analysis of C and N; (c) C 1s and (d) N 1s XPS spectra of pCNTAs. Effects of plasma treatment on the component percentage of CNTA and pCNTAs: (e) XPS spectra, (f) Raman spectra.

41]. After plasma treatment, a new peak at 288.3 eV appears assigned to C=O, which can be attributed to the oxidation of the freshly-treated pCNTA after exposure in air. As for N 1s spectra, only two peaks can be found in Fig. 2d, i.e., peak at 398.5 eV for pyridinic N and peak at 400.5 eV for pyrrolic N [23,42,43]. Obviously, the N content decreases with long-time plasma treatment.

The investigation on the variation of each component under different plasma treatment times shows that the percentage of each component does not change linearly with the treatment condition. The variation is selectively summarized in Fig. 2e. The percentage of pyrrolic N decreases first, and then increases. While the percentage of pyridinic N is just the opposite. An inflection point appears at pCNTA10. Additionally, the ratio of I_D/I_G in the Raman spectra rises with the treatment time prolonging, indicating the increase of the defect structure after plasma treatment (Fig. 2f and Fig. S4). Further

analysis indicates that the percentage of N doping and defects of carbon outside the sp^2 plane present a similar variation to that observed from XPS. The percentage of N doping first rises then falls, and that of carbon outside sp^2 plane is on the contrary. The inflection points of them both appear at pCNTA10.

Considering the special feature of pCNTA10, we first compared the electrochemical CO_2RR performances of CNTA and pCNTA10. The corresponding electrochemical performances were measured in a standard three-electrode system in 0.5 mol L^{-1} $NaHCO_3$. The linear scan voltammetry (LSV) curve of CNTA in CO_2-saturated electrolyte shows a much larger current than that in Ar (Fig. 3a). After plasma treatment, the current density of pCNTA10 further increases. With CO_2 bubbling, two gaseous products, H_2 and CO, can be detected for both CNTA and pCNTA10 by gas chromatography (GC) (Figs S5, S6). No liquid product is detected. And −0.82 V *vs.* reversible hydrogen electrode (RHE) is the optimal potential for CO production (Fig. 3b). Specifically, the CO FE of pCNTA10 at −0.82 V is up to 75 %, obviously higher than that of CNTA (53%). The CO production rate of pCNTA10 at −0.82 V is 0.252 mmol cm^{-2} h^{-1}, also higher than that of CNTA of 0.135 mmol cm^{-2} h^{-1} (Fig. 3c). Besides, both CNTA and pCNTA10 exhibit excellent FE stability and current density stability at −0.82 V for over 10 h (Fig. 3d and Fig. S7). Additionally, the carbon source of CO in the product was investigated through the isotope labelling experiment (Fig. 3e). By using $^{13}CO_2$ as the feedstock, a strong peak at *m*/*z* of 29 attributed to ^{13}CO can be found in the GC-mass spectrum (GC-MS), demonstrating that the obtained CO is from CO_2 rather than the electrolyte or the decomposition of the catalyst. Furthermore, *in situ* potential-dependent attenuated total reflectance-Fourier transform infrared (ATR-FTIR) spectroscopy was employed to probe the reaction path over CNTA and pCNTA10 (Fig. 3f–g). CNTA and pCNTA10 show similar spectra. The band at 1635 cm^{-1} is attributed to interfacial water [44]. While the band at 1400 cm^{-1} represents the absorption of *COOH [45,46], indicating the formation of CO is with *COOH as the intermediate. The *COOH intensity of pCNTA10 is slightly stronger than that of CNTA, reflecting that the plasma treatment is beneficial to the selectivity to CO.

The CO_2RR activity of all the plasma-treated samples with CNTA (Fig. 4a) was investigated, showing only CO and H_2 as the products. And the optimal potential for CO is −0.82 V for all the samples as well. Among all the plasma-treated samples, pCNTA10 performs the highest FE of CO. Given the special place of pCNTA10 in the

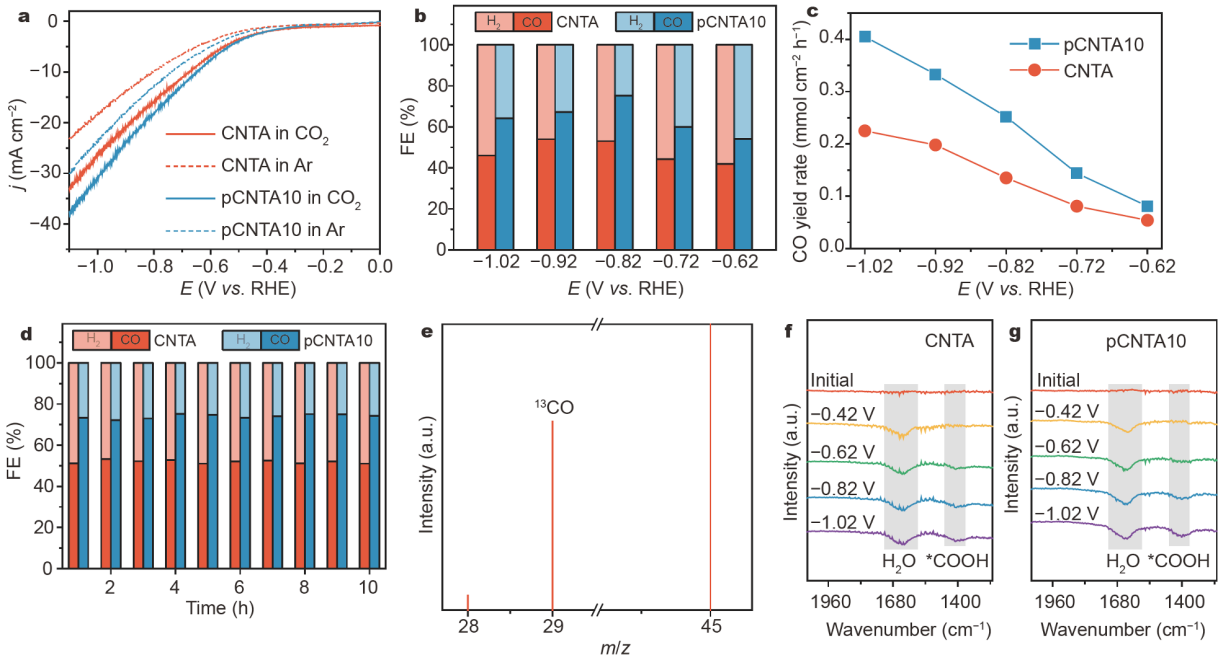

Figure 3 (a) LSV curves of CNTA and pCNTA10 under Ar and CO_2, respectively. (b) FEs of CNTA and pCNTA10 under different potentials. (c) CO production rates of CNT and pCNTA10 under different potentials. (d) FE stability of CNTA and pCNTA10 at −0.82 V. (e) GC-MS spectrum of the gaseous products of pCNTA10 by using $^{13}CO_2$ as the feedstock. The peak at 28 corresponds to ^{12}CO resulting from inevitable $^{12}CO_2$ in the system. And the peak at 45 represents the $^{13}CO_2$ as the feedstock. (f, g) *In situ* potential-dependent ATR-FTIR spectra of (f) CNTA and (g) pCNTA10.

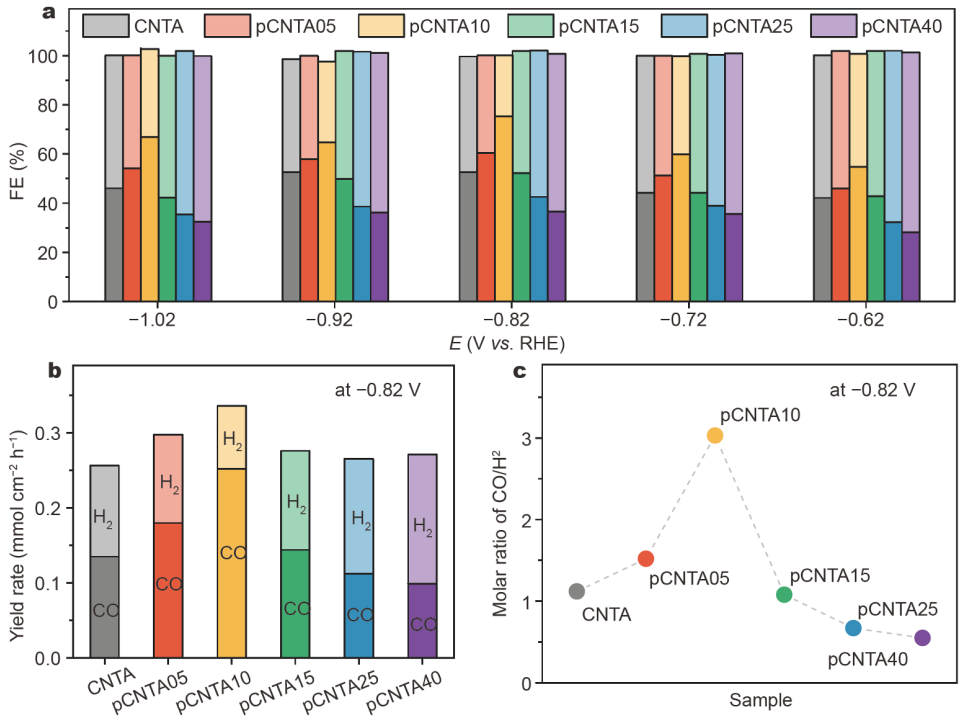

Figure 4 (a) FEs of CNTA and pCNTAs at given potentials. Light-colored column and dark-colored column represent H_2 and CO, respectively. (b) Yield rates of syngas and (c) molar ratio of CO/H_2 over CNTA and pCNTAs at −0.82 V.

structure variation (Fig. 2e–f), it can be speculated from the results of XPS that the pyridinic N facilitates the formation of CO, while pyrrolic N is in favor of HER. As for the results from Raman spectra, N doping, especially pyridinic N as indicated by XPS, is beneficial to CO_2RR, and the carbon outside the sp^2 plane is on the contrary. Furthermore, at −0.82 V, all the samples show a similar total syngas yield rate of around 0.3 mmol cm^{-2} h^{-1} (Fig. 4b), and the corresponding CO/H_2 ratios range from 0.55 to 3.03 (Fig. 4c), which is suitable for the downstream Fischer-Tropsch synthesis [47]. As a result, the syngas with a tunable CO/H_2 ratio can be simply adjusted through Ar-plasma treatment with different conditions.

In our case, although altering the applied potential can also adjust the CO/H_2 ratio of the generated syngas, the huge difference in the yield rate at different potentials will severely limit the potential practical application (Fig. S8). With the facile treatment of Ar plasma, the syngas with different CO/H_2 ratios can be acquired at the close yield rate. Besides, CNTA contains the necessary components for both HER and CO_2RR. And the plasma treatment on CNTA leads to a synchronous change on these components, providing an opportunity to simultaneously manipulate the reaction rate of HER and CO_2RR. Additionally, plasma treatment also introduces many exposed edge sites, making pCNTA more active for CO_2RR [48]. In this way, the resulting CO/H_2 ratio can be further expanded.

In summary, we demonstrate the facile Ar-plasma treatment to CNTA as electrocatalyst to efficiently generate the syngas with a controllable CO/H_2 ratio. Under Ar-plasma treatment for 10 min, the pCNTA10 exhibits the highest CO FE of 75% with stability for more than 10 h. By changing the treatment conditions, the CO/H_2 ratio can be regulated between 0.55 and 3.03, which is capable of Fischer-Tropsch synthesis. Combining the results of structural variation and the results of FE, it can be deduced that pyridinic N is advantageous for the formation of CO, while pyrrolic N and carbon outside the sp^2 plane are in favor of HER. Our work not only reveals the relationship between the structure and the CO_2RR activity of CNTA, but also opens up a new path for efficient production of syngas with a tunable ratio of CO/H_2.

Received 9 March 2020; accepted 16 May 2020; published online 17 July 2020

1 Jiao F, Li J, Pan X, *et al.* Selective conversion of syngas to light olefins. Science, 2016, 351: 1065–1068
2 Zhong L, Yu F, An Y, *et al.* Cobalt carbide nanoprisms for direct production of lower olefins from syngas. Nature, 2016, 538: 84–87

3 Zhu Y, Pan X, Jiao F, *et al.* Role of manganese oxide in syngas conversion to light olefins. ACS Catal, 2017, 7: 2800–2804
4 Luk HT, Mondelli C, Ferré DC, *et al.* Status and prospects in higher alcohols synthesis from syngas. Chem Soc Rev, 2017, 46: 1358–1426
5 Lv K, Teng C, Shi M, *et al.* Hydrophobic and electronic properties of the e-MoS_2 nanosheets induced by FAS for the CO_2 electroreduction to syngas with a wide range of CO/H_2 ratios. Adv Funct Mater, 2018, 28: 1802339
6 Hernández S, Amin Farkhondehfal M, Sastre F, *et al.* Syngas production from electrochemical reduction of CO_2: current status and prospective implementation. Green Chem, 2017, 19: 2326–2346
7 He Q, Liu D, Lee JH, *et al.* Electrochemical conversion of CO_2 to syngas with controllable CO/H_2 ratios over Co and Ni single-atom catalysts. Angew Chem Int Ed, 2020, 59: 3033–3037
8 Guo S, Zhao S, Wu X, *et al.* A Co_3O_4-CDots-C_3N_4 three component electrocatalyst design concept for efficient and tunable CO_2 reduction to syngas. Nat Commun, 2017, 8: 1828
9 Ross MB, Dinh CT, Li Y, *et al.* Tunable Cu enrichment enables designer syngas electrosynthesis from CO_2. J Am Chem Soc, 2017, 139: 9359–9363
10 Zheng T, Jiang K, Ta N, *et al.* Large-scale and highly selective CO_2 electrocatalytic reduction on nickel single-atom catalyst. Joule, 2019, 3: 265–278
11 Jiang K, Siahrostami S, Zheng T, *et al.* Isolated Ni single atoms in graphene nanosheets for high-performance CO_2 reduction. Energy Environ Sci, 2018, 11: 893–903
12 Li YC, Wang Z, Yuan T, *et al.* Binding site diversity promotes CO_2 electroreduction to ethanol. J Am Chem Soc, 2019, 141: 8584–8591
13 Wang YR, Huang Q, He CT, *et al.* Oriented electron transmission in polyoxometalate-metalloporphyrin organic framework for highly selective electroreduction of CO_2. Nat Commun, 2018, 9: 4466
14 Zhu Q, Ma J, Kang X, *et al.* Electrochemical reduction of CO_2 to CO using graphene oxide/carbon nanotube electrode in ionic liquid/acetonitrile system. Sci China Chem, 2016, 59: 551–556
15 Zhang H, Li J, Xi S, *et al.* A graphene-supported single-atom FeN_5 catalytic site for efficient electrochemical CO_2 reduction. Angew Chem Int Ed, 2019, 58: 14871–14876
16 Lee JH, Kattel S, Jiang Z, *et al.* Tuning the activity and selectivity of electroreduction of CO_2 to synthesis gas using bimetallic catalysts. Nat Commun, 2019, 10: 3724
17 Yang D, Zhu Q, Sun X, *et al.* Electrosynthesis of a defective indium selenide with 3D structure on a substrate for tunable CO_2 electroreduction to syngas. Angew Chem Int Ed, 2020, 59: 2354–2359
18 Vasileff A, Zheng Y, Qiao SZ. Carbon solving carbon's problems: Recent progress of nanostructured carbon-based catalysts for the electrochemical reduction of CO_2. Adv Energy Mater, 2017, 7: 1700759
19 Hu C, Dai L. Doping of carbon materials for metal-free electrocatalysis. Adv Mater, 2019, 31: 1804672
20 Pan F, Li B, Xiang X, *et al.* Efficient CO_2 electroreduction by highly dense and active pyridinic nitrogen on holey carbon layers with fluorine engineering. ACS Catal, 2019, 9: 2124–2133
21 Han H, Park S, Jang D, *et al.* Electrochemical reduction of CO_2 to CO by N,S dual-doped carbon nanoweb catalysts. ChemSusChem, 2020, 13: 539–547
22 Sreekanth N, Nazrulla MA, Vineesh TV, *et al.* Metal-free boron-doped graphene for selective electroreduction of carbon dioxide to formic acid/formate. Chem Commun, 2015, 51: 16061–16064
23 Zhang B, Zhang J, Zhang F, *et al.* Selenium-doped hierarchically porous carbon nanosheets as an efficient metal-free electrocatalyst for CO_2 reduction. Adv Funct Mater, 2019, 30: 1906194
24 Wu J, Ma S, Sun J, *et al.* A metal-free electrocatalyst for carbon dioxide reduction to multi-carbon hydrocarbons and oxygenates. Nat Commun, 2016, 7: 13869
25 Sharma PP, Wu J, Yadav RM, *et al.* Nitrogen-doped carbon nanotube arrays for high-efficiency electrochemical reduction of CO_2: On the understanding of defects, defect density, and selectivity. Angew Chem Int Ed, 2015, 54: 13701–13705
26 Li Q, Zhu W, Fu J, *et al.* Controlled assembly of Cu nanoparticles on pyridinic-N rich graphene for electrochemical reduction of CO_2 to ethylene. Nano Energy, 2016, 24: 1–9
27 Liu S, Yang H, Huang X, *et al.* Identifying active sites of nitrogen-doped carbon materials for the CO_2 reduction reaction. Adv Funct Mater, 2018, 28: 1800499
28 He C, Zhang Y, Zhang Y, *et al.* Molecular evidence for metallic cobalt boosting CO_2 electroreduction on pyridinic nitrogen. Angew Chem Int Ed, 2020, 59: 4914–4919
29 Liu R, Wang Y, Liu D, *et al.* Water-plasma-enabled exfoliation of ultrathin layered double hydroxide nanosheets with multivacancies for water oxidation. Adv Mater, 2017, 29: 1701546
30 Zhang C, Huang Y, Yu Y, *et al.* Sub-1.1 nm ultrathin porous CoP nanosheets with dominant reactive {200} facets: a high mass activity and efficient electrocatalyst for the hydrogen evolution reaction. Chem Sci, 2017, 8: 2769–2775
31 Bharti B, Kumar S, Lee HN, *et al.* Formation of oxygen vacancies and Ti^{3+} state in TiO_2 thin film and enhanced optical properties by air plasma treatment. Sci Rep, 2016, 6: 32355
32 Dou S, Tao L, Wang R, *et al.* Plasma-assisted synthesis and surface modification of electrode materials for renewable energy. Adv Mater, 2018, 30: 1705850
33 Chen C, Tao L, Du S, *et al.* Advanced exfoliation strategies for layered double hydroxides and applications in energy conversion and storage. Adv Funct Mater, 2020, 30: 1909832
34 Xu L, Jiang Q, Xiao Z, *et al.* Plasma-engraved Co_3O_4 nanosheets with oxygen vacancies and high surface area for the oxygen evolution reaction. Angew Chem Int Ed, 2016, 55: 5277–5281
35 Zhang Y, Xu Z, Li G, *et al.* Direct observation of oxygen vacancy self-healing on TiO_2 photocatalysts for solar water splitting. Angew Chem Int Ed, 2019, 58: 14229–14233
36 Balandin AA, Ghosh S, Bao W, *et al.* Superior thermal conductivity of single-layer graphene. Nano Lett, 2008, 8: 902–907
37 Mukherjee S, Cullen DA, Karakalos S, *et al.* Metal-organic framework-derived nitrogen-doped highly disordered carbon for electrochemical ammonia synthesis using N_2 and H_2O in alkaline electrolytes. Nano Energy, 2018, 48: 217–226
38 Wu G, Johnston CM, Mack NH, *et al.* Synthesis–structure–performance correlation for polyaniline–Me–C non-precious metal cathode catalysts for oxygen reduction in fuel cells. J Mater Chem, 2011, 21: 11392–11405
39 Li H, Xiao N, Wang Y, *et al.* Nitrogen-doped tubular carbon foam electrodes for efficient electroreduction of CO_2 to syngas with potential-independent CO/H_2 ratios. J Mater Chem A, 2019, 7: 18852–18860
40 Kuang M, Guan A, Gu Z, *et al.* Enhanced N-doping in mesoporous carbon for efficient electrocatalytic CO_2 conversion. Nano Res, 2019, 12: 2324–2329
41 Hursán D, Samu AA, Janovák L, *et al.* Morphological attributes

govern carbon dioxide reduction on N-doped carbon electrodes. Joule, 2019, 3: 1719–1733
42 Wang H, Chen Y, Hou X, *et al.* Nitrogen-doped graphenes as efficient electrocatalysts for the selective reduction of carbon dioxide to formate in aqueous solution. Green Chem, 2016, 18: 3250–3256
43 Jhong HRM, Tornow CE, Smid B, *et al.* A nitrogen-doped carbon catalyst for electrochemical CO_2 conversion to CO with high selectivity and current density. ChemSusChem, 2017, 10: 1094–1099
44 Katayama Y, Nattino F, Giordano L, *et al.* An *in situ* surface-enhanced infrared absorption spectroscopy study of electrochemical CO_2 reduction: Selectivity dependence on surface C-bound and O-bound reaction intermediates. J Phys Chem C, 2018, 123: 5951–5963
45 Firet NJ, Smith WA. Probing the reaction mechanism of CO_2 electroreduction over Ag films *via operando* infrared spectroscopy. ACS Catal, 2017, 7: 606–612
46 Meng N, Liu C, Liu Y, *et al.* Efficient electrosynthesis of syngas with tunable CO/H_2 ratios over $Zn_xCd_{1-x}S$-amine inorganic-organic hybrids. Angew Chem Int Ed, 2019, 58: 18908–18912
47 Meng N, Zhou W, Yu Y, *et al.* Superficial hydroxyl and amino groups synergistically active polymeric carbon nitride for CO_2 electroreduction. ACS Catal, 2019, 9: 10983–10989
48 Shen A, Zou Y, Wang Q, *et al.* Oxygen reduction reaction in a droplet on graphite: Direct evidence that the edge is more active than the basal plane. Angew Chem Int Ed, 2014, 53: 10804–10808

Acknowledgements We acknowledge the National Natural Science Foundation of China (21871206 and 21901180), and China Postdoctoral Science Foundation (2019TQ0226) for the financial support.

Author contributions Zhang B conceived and directed the project. Ji Y carried out the experiments. Shi Y analyzed the data and wrote the paper. Zhang B and Liu C revised the paper. All authors contributed to the general discussion.

Conflict of interest The authors declare no conflict of interest.

Supplementary information Experimental details and supplementary figures are available in the online version of the paper.

Yan Ji received his BSc degree from Tianjin Normal University in 2017. Currently, he is a Master candidate at Tianjin University under the supervision of Prof. Bin Zhang. His research topic is the development of non-noble metal electrocatalysts for CO_2RR.

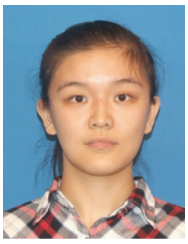

Yanmei Shi received her PhD degree from Tianjin University in 2018 (supervised by Prof. Bin Zhang). She is currently conducting postdoctoral research at Tianjin University (with Prof. Bin Zhang). Her research focuses on exploring structural reconstruction and active species of catalytic materials under electrocatalytic conditions.

Bin Zhang received his PhD degree from the University of Science and Technology of China in 2007 (supervised by Prof. Yi Xie). He carried out postdoctoral research at the University of Pennsylvania (July 2007 to July 2008, with Prof. Ritesh Agarwal) and worked as an Alexander von Humboldt fellow at Max Planck Institute of Colloids and Interfaces (August 2008 to July 2009, with Dayang Wang). Currently, he is a Fellow of the Royal Society of Chemistry (FRSC), and a professor at Tianjin University and the Collaborative Innovation Center of Chemical Science and Engineering (Tianjin). His research mainly focuses on the controlled chemical transformation synthesis of advanced nanomaterials for catalytic applications.

等离子体处理的氮掺杂碳纳米管阵列用于电化学CO_2还原制备比例可控的合成气

纪岩[1], 史艳梅[1*], 刘翠波[1], 张兵[1,2*]

摘要 合成气是一种CO和H_2的混合气，是工业上生产烯烃、液体燃料、聚合物、药物等产品的重要原料. 通过电化学还原的方法将CO_2转化为合成气，不仅能够减少大气中的CO_2含量，同时还能缓解能源危机. 但是目前仍然缺乏廉价高效的电催化剂来实现可控比例CO/H_2的合成. 因此，我们发展了一种简易的等离子体处理策略，利用氮掺杂碳纳米管阵列作为电催化剂，通过电化学CO_2-H_2O还原制备CO/H_2比例可控的合成气. 在不同的等离子体处理条件下，CO/H_2比例的范围可达0.55–3.03，符合下游化工生产的原料气标准. 通过优化等离子体处理条件，CO的法拉第效率最高可达75%，并且能够维持稳定性长达10 h. 通过研究氮掺杂的碳纳米管的结构随处理条件的变化，并结合其CO_2还原活性，我们推断出氮掺杂碳纳米管中的吡啶氮有利于CO_2转化为CO，而吡咯氮和sp^2平面外的碳则有利于氢气的产生. 利用等离子体处理的方法能够有效调节催化剂中各活性组分的比例，从而调控CO_2还原反应和析氢反应的速率，最终实现CO/H_2比例可控的合成气制备.

